20 mlb (nominal); 2) specific impulse, 5000 sec; 3) power requirement, 4 kw; 4) system weight, 98 lb; 5) propellant weight per 180 days (i.e., possible resupply period) 60 lb; 6) size (including propellant): diameter, 12 in.; and length, 24 in.

Conclusions

The high specific impulse ion engine has been shown to be strongly competitive with chemical rockets for applications such as the attitude control and station keeping of synchronous satellites. The ion-propulsion control system offers advantages over other contemporary control systems both in total system weight and precision control. These advantages extend to other satellite control applications such as orbit maintenance for nonsynchronous medium-altitude satellites and manned space stations. For most satellite control applications, the power required to operate the ion engine is less than a few kilowatts (usually on the order of 100–1000 w) and can be supplied, therefore, by solar cells. Ion-engine efficiencies and lifetimes have already reached levels that satisfy most satellite control requirements. Furthermore, demonstration of an operating prototype of a satellite control system has shown that such systems can be reduced to engineering practice. For these reasons, ion propulsion can be given serious consideration for near-future satellite control applications.

References

[1] Work, G. A., Molitor, J. H., Kaplan, M. H., and Collett, C. R., "Design and performance of ion engine systems for control of earth satellites," AIAA Preprint 64-501 (June 1964).

[2] Molitor, J. H. and Kaplan, M. H., "Optimization of ion engine control systems for synchronous satellites," J. Spacecraft Rockets **1**, 557–559 (1964).

[3] Ehricke, K. A., "Dynamics," *Space Flight* (D. Van Nostrand Co., Inc., Princeton, N. J., 1962), Vol. II, pp. 144–150.

[4] Kaplan, M. H., Molitor, J. H., and Buckey, C. R., "The perturbed and corrected motion of earth satellites," Hughes Research Labs., Research Rept. 320 (September 1964).

[5] Molitor, J. H., "Ion propulsion system for stationary-satellite control," J. Spacecraft Rockets **1**, 170–175 (1964).

[6] Roach, R. D., Jr., "Rocket type reaction control systems for spacecraft," Society of Automotive Engineers A6-D Committee Meeting, Phoenix, Ariz. (September 26, 1961).

[7] Karrenberg, H. K. and Luders, R. D., "Orbital aspects of non-synchronous communication satellite systems," AIAA Preprint 63-397 (August 1963); also *AIAA Progress in Astronautics and Aeronautics: Celestial Mechanics and Astrodynamics*, edited by V. G. Szebehely (Academic Press Inc., New York, 1964), Vol. 14, pp. 203–255.

SEPT.-OCT. 1965 J. SPACECRAFT VOL. 2, NO. 5

Development Status of Low-Power Arc-Jet Engines

WILLIAM A. GEIDEMAN JR.* AND KURT MULLER†
Giannini Scientific Corporation, Santa Ana, Calif.

The results of a continuous performance test of a 2-kw arc-jet thrustor are presented. The design concepts that were employed to obtain the thrustor design are covered in some detail. This thrustor is a revised version of an earlier 1-kw thrustor design. In addition, the results of a pulsed-mode test on a 1-kw thrustor are presented. A continuous lifetime of 150 hr without failure of the thrustor has been demonstrated. This same thrustor has been operated at specific impulse levels as high as 1270 sec and at input power levels up to 3.5 kw. In the pulsed-mode operation, 17,580 hot thrust pulses were achieved in the test.

Nomenclature

a, A	=	area, m^2, ft^2
F	=	thrust, lb, newton
f	=	friction force, newton
i	=	specific enthalpy, joule/kg°C
I_{sp}	=	specific impulse, sec
m	=	$\tan\gamma$
$\dot{m}$	=	mass flow, lb/sec, kg/sec
M	=	momentum, newton
p	=	pressure, newton/m^2, in Hg
R, U, V, W	=	dimensionless parameters, Eq. (3)
Re	=	Reynolds number
r	=	radius, m
t	=	time, sec
T	=	temperature, °K
u	=	velocity, m/sec, fps
v	=	specific volume, m^3/kg
x, y, ξ, η	=	Cartesian coordinates
γ	=	angle, isentropic exponent
ϵ	=	momentum ratio [see Eq. (19)]
λ_f	=	friction coefficient
ρ	=	density, kg/m^3
μ	=	absolute viscosity, kg/sec-m
θ	=	nozzle divergence half angle
ψ	=	density ratio, ρ/ρ_c
A^*	=	dimensionless parameter, Eq. (5)
ϕ, Ω	=	dimensionless parameters, Eq. (13)

Subscripts

c	=	nozzle chamber
e	=	nozzle exit
is	=	isentropic
o	=	origin
st	=	stagnation
th	=	nozzle throat

Presented as Preprint 64-502 at the 1st AIAA Annual Meeting, Washington, D. C., June 29–July 2, 1964; revision received March 4, 1965. Most of the analytical and experimental results presented herein were obtained under the sponsorship of NASA Lewis Research Center, Contract No. NAS 3-2521.

* Engineering Specialiist; now Senior Physicist, Systems Department, Spectrolab Division of Textron Electronics, Sylmar, Calif. Member AIAA.

† Senior Engineer; now Senior Physicist, Systems Department, Spectrolab Division of Textron Electronics, Sylmar, Calif.

Introduction

STUDIES have shown that electrothermal thrustors, typified by the arc-jet and resistojet, are suitable for a variety of early space applications.[1,2] This paper considers

the evolution and development of a low-power (2-kw) arc-jet thrustor. Earlier efforts related to a 1-kw arc-jet thrustor have been reported previously.[3,4] The efforts described herein were oriented toward a 2-kw thrustor in an effort to alleviate problems associated with life and low Reynolds numbers by increasing the over-all thrustor size.

Although the ultimate application for this thrustor would undoubtedly require pulsed-mode operation, it was believed necessary to demonstrate that long life under continuous operating conditions could be achieved prior to initiating intensive studies of pulsed-mode operation. A parametric study of specific geometric variables and operating conditions was undertaken to ascertain their effects on performance and life. These studies resulted in a 2-kw continuous arc-jet thrustor that demonstrated life in excess of 150 hr at a specific impulse of 935 sec and thrust of 30.1 mlb. This thrustor was operated successfully for short periods at specific impulse levels to 1275 sec and at power levels from 1.5 to 3.5 kw. Preliminary studies were also performed on a 1-kw thrustor to determine its performance during pulsed-mode operation. This test (~200-msec pulses) was reasonably successful and indicated the potential for development of arc-jet thrustors for this operational mode. Such thrustors could find applications in several early space missions, such as long-duration attitude control and orbit correction for communication satellites, geophysical satellites, and manned orbiting space stations.

Design and Development of 2-kw Continuous Arc-Jet Thrustor

The basic design was derived from the concept used in the previous 1-kw arc-jet program. Figure 1 shows the configuration used during the first phase of the program. The thrustor was radiation-cooled. The arc was constricted and stabilized by means of a vortex. The discharge passed completely through the throat and the arc foot attached in the divergent section of the nozzle. This particular arc configuration in conjunction with radiation cooling was found to be attractive in terms of efficiency and specific impulse for the desired power level. Weight and dimensions were not optimized for the experimental unit in order to minimize the gas seal problem.

An interchangeable anode insert was used to permit easy modification of electrode and nozzle geometry. The thoriated tungsten anode insert was held in position in the molybdenum housing by the wedge action of a 3-deg taper, which was found experimentally to produce a firm and gas-tight connection. The thoriated tungsten cathode was inserted into the boron nitride cathode insulator, which was pressed into the precision bore of the housing. The gap between the anode and cathode could be adjusted over a wide range.

The propellant entered the thrustor through the side port and was guided by four holes from the outer ring chamber to the center bore in the cathode insulator. From there it flowed axially through the annular passage formed by the cathode and cathode insulator to the threaded passage, which induced a vortex flow in the constrictor.

The first part of the program was devoted to comprehensive parametric studies of geometric and operating variables and their effect on I_{sp}, efficiency, and life. The throat diameter, throat length, nozzle divergence half angle, nozzle area ratio, cathode-anode gap, propellant flow, and input power were the subjects of experimental and theoretical investigations.

During the course of the program, it became evident that the thrustor shown in Fig. 1 was deficient in three major areas: the vortex generation of the propellant, the geometry of the anode nozzle, and the heat-transfer mechanism from the hot-spot region to the radiating areas. Therefore, the thrustor was redesigned. A cross-sectional drawing of the improved design is shown in Fig. 2. The incoming propellant is ducted through the trapezoidal thread on the outside of the

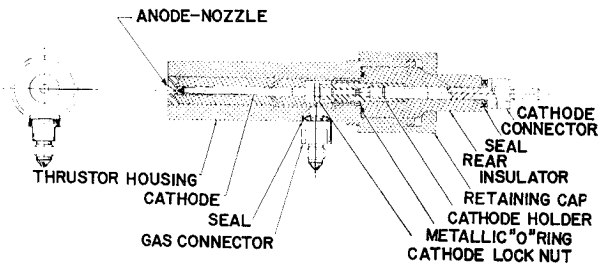

Fig. 1 Original thrustor design.

cathode insulator toward the outer annular receiver. The gas from the receiver is injected tangentially through six holes into the inner annular chamber that functions as a vortex chamber. Some axial velocity was imparted by inclining the injector holes. The propellant flows from the vortex chamber to the throat through the coaxial conical passage formed by the inlet section of the anode and the tip of the cathode. The new anode insert was designed specifically to increase the heat flux to the radiating areas. The enlarged disk acted as a radiator. Some of the facts that led to the new design are described in the following sections.

Flow through Thrustor

In small arc-jet thrustors, the anode and cathode cooling problems are unusually difficult because of the small propellant flow rates employed. The heat input to the electrodes tends to increase as the thrustor size is reduced. Furthermore, the relative surface roughness (the ratio of surface finish to diameter of the passage) increases drastically resulting in high friction losses and decay of the vortex. The problem was attacked both analytically and experimentally in an effort to provide a better understanding of the nature of the flow patterns and heat-transfer mechanisms.

The first step was to establish the flow sections between the cathode and anode. They are formed by two concentric cones whose generating lines are a for the anode and c for the cathode (Fig. 3). The flow area with respect to the point P_0 on a is the minimum surface of a frustum defined by P_0, P, and the generating line d (cf. Fig. 3). Thus the problem may be formulated as one of finding the half angle γ, which produces the smallest frustum for a given point P_0.

The flow area may be calculated by

$$a = \pi(y_0 + \eta)[(\xi - x_0)^2 + (\eta - y_0)^2]^{1/2} \qquad (1)$$

where $\xi = \xi(\gamma)$, and $\eta = \eta(\gamma)$. Using the notation $\tan\gamma = m$ and $\tan\gamma_0 = m_0$, the angle γ defining the position of the minimum flow area was derived from the following equation:

$$(d/dm)[a(m)] = 0 \qquad (2)$$

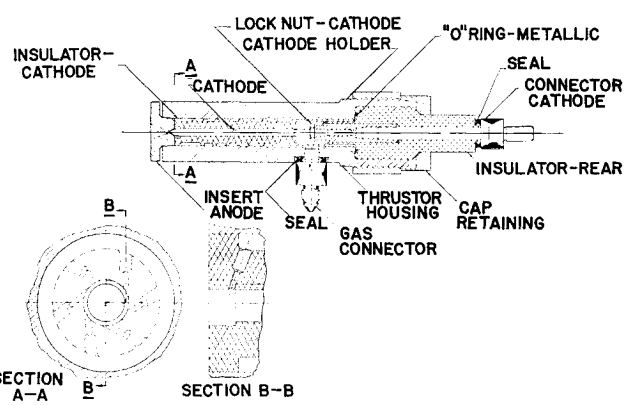

Fig. 2 New thrustor design.

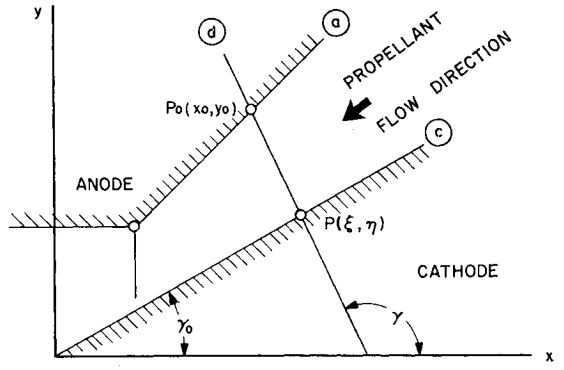

Fig. 3 Flow passage in the constrictor inlet section.

With the following substitutions:

$$\left.\begin{aligned} R &= x_0/y_0 \qquad U = 2m_0R(m_0R - 1) \\ V &= m^2R^2 - 2m_0^2(m_0R - 1) - 1 \\ W &= 3m_0 - 4m_0^2R + m_0^3R^2 \end{aligned}\right\} \tag{3}$$

the solution of Eq. (2) was found to be

$$m = [-V + (V^2 - 4UW)^{1/2}]/2U \tag{4}$$

and the area expressed in dimensionless form became

$$A^* = \frac{a}{y_0^2} = \pi\left[\frac{m_0}{m_0 - m}(1 - mR) + 1\right] \times \left\{\left[\frac{1}{m_0 - m}(1 - mR) - R\right]^2 + \left[\frac{m_0}{m_0 - m}(1 - mR) - 1\right]^2\right\}^{1/2} \tag{5}$$

A typical curve showing the flow sections in the constrictor inlet region, throat, and diffuser is presented in Fig. 4b. The flow pattern in the constrictor inlet region consists of axial flow with a swirl superimposed. In the throat and particularly in the nozzle sections the tangential flow component becomes small compared to the axial component; hence, it was neglected. However, in the constricted inlet region, both of the flow vectors are of the same order, and it was found necessary to use the vector sum of the two components to arrive at realistic friction losses and to gain more insight into heat-transfer phenomena.

The determination of the tangential flow component requires knowledge of the vortex pattern. The simplest model of a vortex is known as the combined vortex, from Rankine,[5] which consists of a central rotational zone of constant vorticity, in which the velocity varies in proportion to the radial distance from the axis, and a surrounding irrotational zone of constant circulation, in which the velocity varies inversely with the radius. Since friction losses in small thrustors become more pronounced, the dissipation of the vortex energy is an essential factor and can no longer be disregarded. Examination of the viscous and shear forces occurring in the passages indicated that the actual vortex pattern differed significantly from the Rankine model. In view of these circumstances an attempt has been made to estimate the velocity field by making an arbitrary assumption that half of the original kinetic energy is dissipated before the vortex is formed, and, thereafter, the vortex motion follows the structure of Rankine's combined vortex model. This method is highly artificial, except for velocities near the axis. Nevertheless, the scheme described previously was applied to conduct studies on different inlet geometries, and it proved to be useful in providing a basis for understanding the electrode cooling phenomena and arc stabilization. From the cooling and stabilization point of view, it was desirable to choose the geometry presented in Fig. 4a.

The axial flow pattern and pressure distribution were calculated using classical gas dynamics. Although partial ionization and frozen flow phenomena require a more detailed analysis of the problem, the assumption of uniform flow in equilibrium condition was sufficient to provide guidance for experimental investigations. The idealized thermodynamic process of an arc-jet engine is shown schematically in the enthalpy-entropy diagram of Fig. 5.

The numerical subscripts refer to the locations shown in Fig. 4a by the numbers 3, 4, 5′, 5″, and 6. The gas is assumed to expand isentropically from the vortex chamber (location 3) to the smallest flow section (location 4). If the cathode tip protrudes into the inlet section of the throat, the flow area increases after the minimum flow section causing some compression of the gas caused by the diffusing action of the passage. The heat is added to the propellant between the locations 5′ and 5″. The expansion of the gas takes place between 5″ and 6. The velocity, pressure, and Reynolds number are plotted in Fig. 4c. The result is typical of a thrustor operating at a specific impulse of 1000 sec, 2-kw input power, 2×10^{-5} lb/sec hydrogen mass flow, and 30% thermal efficiency. The Reynolds numbers throughout are in the laminar range.

Geometry of Anode Nozzle

The thrust efficiency depends to a large extent upon the nozzle performance. The governing parameters of a nozzle are the divergence half angle and the exit area ratio. In the previous 1-kw arc-jet program, it was believed that nozzles operating in the laminar flow regime should be designed with a low area ratio $A_e/A_{th} < 10$ and a divergence half angle $\theta > 30°$. Since short nozzles with a large divergence resulted in moderate nozzle efficiencies, the nozzle concept was revised.

A complete analysis of nozzles utilized in electric propulsion devices should include two-dimensional flow, atomic and ionic recombination, flow rotation, flow separation, friction, heat transfer between the propellant and nozzle walls, and the nonuniform temperature profiles of the gas column. Some of the factors listed previously are of first-order influence, and some have a secondary effect on the nozzle performance. Considerable effort has been expended in the past to analyze the problem thoroughly. Because of the mathematical difficulties encountered in solving the equations which describe the velocity field, a general analytic solution applicable for nozzles in arc-jet engines is not available to date.

The ideal nozzle theory may be applied to match nozzles to the existing operating parameters as a first approximation,

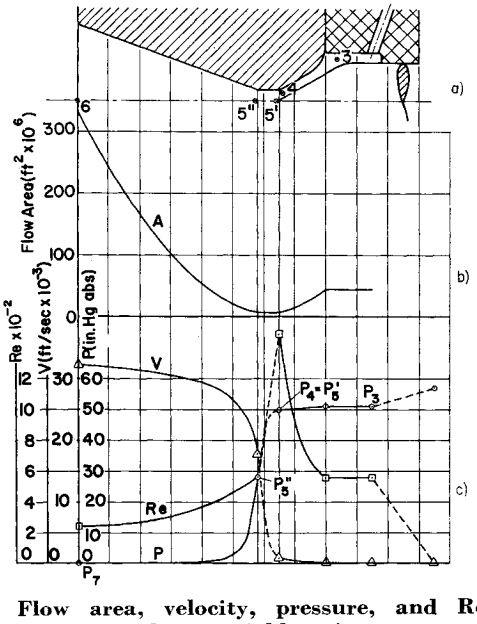

Fig. 4 Flow area, velocity, pressure, and Reynolds number vs axial location.

but the result reveals serious departures from the actual conditions, if any attempt is made to optimize nozzle designs. In order to arrive at concrete results that are applicable to guide experimental testing, the ideal nozzle theory was applied including the effects of viscous friction and nonaxial flow. The result is restricted to conical nozzles, and no attempt has been made to find the optimum contour or shape. Furthermore, the flow pattern at any location on the nozzle axis was assumed to be parabolic. This assumption is very arbitrary, because the flow profile in a diffuser is not parabolic and especially not in an arc-jet nozzle operating in the laminar flow regime. Steep velocity gradients are expected near the diffuser axis because of the high core temperatures. If Newtonian flow is applicable, that is, if the shear stress is proportional to the shear deformation, the model of the parabolic flow pattern should not depart from actual facts completely since the shear deformation du/dr is expected to be of the same order of magnitude. This approximation was sufficient to learn whether short nozzles with a large divergence half angle ($A_e/A_{th} < 10$, $\theta > 30°$) or long nozzles ($A_e/A_{th} > 10$, $20° \leqslant \theta \leqslant 30°$) promise better performance.

A more accurate approach to the optimization of nozzles for arc-jet engines is the method of characteristics combined with boundary-layer theory, since the boundary layer has a significant influence on the shock pattern in the supersonic part of the nozzle. However, this method could not be pursued during the six-month development period because of its time-consuming calculations, since the physical properties of the gas change drastically in both axial and radial directions.

In most cases friction losses are combined with an entropy increase. In this calculation reheating of the gas is neglected; the expansion process was assumed to be isentropic. The result of the calculation is shown in Fig. 6. The square of the quotient of the effective axial exit velocity and ideal velocity is plotted against the exit area ratio. The curves show a marginal increase in the effective exit velocity, if the divergence half angle is larger than 30°, and if the area ratio is larger than 50 at a 30° half angle.

Laminar Friction in a Nozzle

The forces acting on a fluid particle (shown in Fig. 7) are inertia forces, pressure forces, and friction forces. Hence

$$dpA - \rho A\, dx\, du/dt - df = 0 \tag{6}$$

since $v = 1/\rho$ and $u = dx/dt$, Eq. (6) may be written in the following form:

$$vdp - udu - df/\rho A = 0,$$

$$\text{or } di - udu - df/\rho A = 0 \tag{7}$$

Integration of Eq. (7) gives

$$\frac{u^2}{2} - \frac{u_0^2}{2} = i_0 - i_e - \int_0^{x_e} \frac{df}{\rho A} \tag{8}$$

For moderate divergence half angles, the friction force may be approximated by

$$df = A\lambda_f(\rho u^2/2r)dx \tag{9}$$

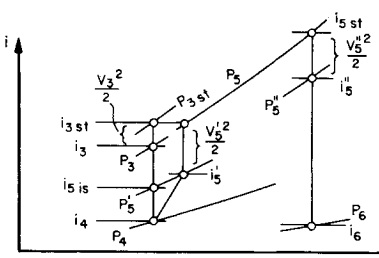

Fig. 5 Enthalpy-entropy diagram for arc heating process.

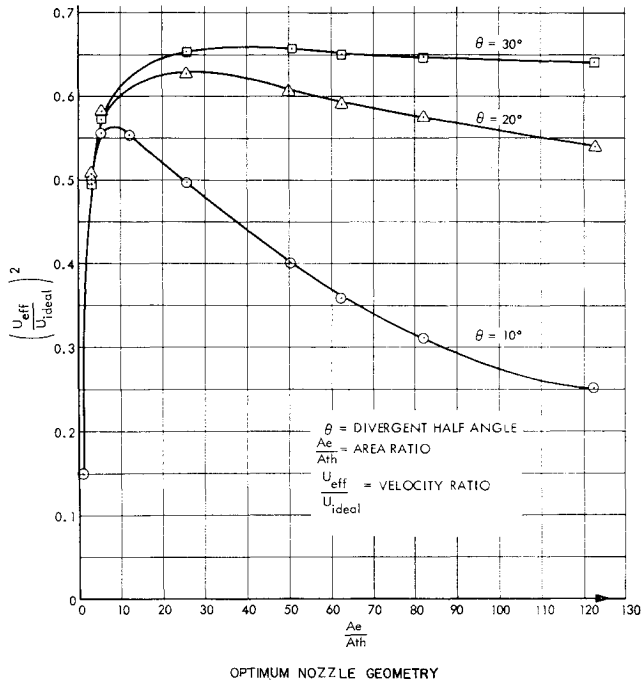

Fig. 6 Exit velocity vs area ratio and divergence half angle.

Using the friction term from Hagen Poiseuille for laminar pipe flow, $\lambda_f = 16/Re$ where $Re = ur\rho/\mu$, and substituting $\dot{m} = \pi r^2 \rho u$, Eq. (9) may be written

$$df/\rho A = (8\mu\dot{m}/\pi r^4\rho^2)dx \tag{10}$$

Thus, the kinetic energy of the gas becomes

$$\frac{u^2}{2} = i_c - i_e - \frac{8\mu\dot{m}}{\pi r_{th}^4 \rho_c^2} \int_0^{x_e} \frac{dx}{(r/r_{th})^4(\rho/\rho_c)^2} \tag{11}$$

The contour of the nozzle is expressed by

$$r/r_{th} = (x/r_{th})\tan\theta + 1 \tag{12}$$

Isentropic expansion is formulated by

$$\psi \equiv \rho/\rho_c = (T/T_c)^{(1/\gamma-1)}$$

After introduction of the energy and mass flow balance and with the notations

$$\left.\begin{aligned} \Omega &\equiv \dot{m}/[\pi r_{th}^2 \rho_c (2c_p T_c)^{1/2}] \\ \phi &\equiv \mu\dot{m}/\Omega^{3/2} r_{th}^3 \rho_c^2 u_{ideal}^2 \end{aligned}\right\} \tag{13}$$

the friction term in Eq. (11) assumes the following form after a variable transformation:

$$\int_0^{x_e} F(x)dx = \frac{r_{th}x}{4\Omega^{3/2}\tan\theta}$$

$$\int_{\psi_{th}}^{\psi_e} [(\gamma^{-1})]\left[\frac{\psi^{\gamma-5/2}}{1-\psi^{\gamma-1}} - 2\psi^{-3/2}\right][1-\psi^{\gamma-1}]^{3/4}d\psi \tag{14}$$

The combination of Eqs. (11) and (14) then yield

$$\left(\frac{u}{u_{ideal}}\right)^2 = 1 - \psi_e{}^{\gamma-1} - \frac{2}{\pi}\frac{\phi}{\tan\theta}\int_{\psi_{th}}^{\psi_e} F(\psi)d\psi \tag{15}$$

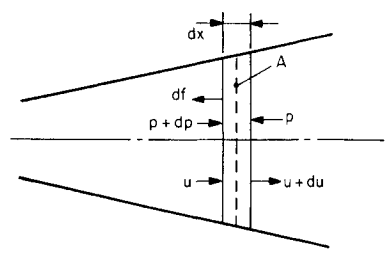

Fig. 7 Forces acting on a fluid particle in the nozzle.

The integral on the right hand side of Eq. (15) was solved numerically by means of a computer taking increments of $\Delta\psi = 0.005$.

The correlation between x and ψ is expressed by

$$x/r_{th} = 1/\tan\theta[(\Omega/\psi)^{1/2}(1 - \psi^{\gamma-1})^{-1/4} - 1] \quad (16)$$

and the area ratio becomes

$$A/A_{th} = r/r_{th}^2 = \Omega/\psi(1 - \psi^{\gamma-1})^{1/2} \quad (17)$$

The boundary conditions are

$$x = 0 \qquad \psi = \psi_{th} = \rho_{th}/\rho_c$$

$$x = x_e \qquad \psi = \psi_e = \rho_e/\rho_c$$

Effects of Nonaxial Flow

The reduction in thrust caused by the presence of nonaxial velocity components in the jet leaving the nozzle is determined by computing the difference between the axial component of momentum flux and the total momentum flux of the jet. The ratio of axial and total momentum is given by

$$M_{axial}/M_{total} = \tfrac{1}{2}(\cos\theta + 1) \quad (18)$$

Since the momentum is proportional to the velocity, Eq. (18) may be written as

$$u_{axial}/u_{total} = \tfrac{1}{2}(\cos\theta + 1) = \epsilon \quad (19)$$

Combining friction and nonaxial flow effects, that is, Eqs. (15) and (19), the effective velocity is derived as follows:

$$u_{eff}/u_{ideal} = \epsilon(u/u_{ideal})_{friction} \quad (20)$$

Experimental results showed that a nozzle with an area ratio of 50 and a 30° half angle was 6% higher in performance than a nozzle with an area ratio of 12 and approximately the same half angle.

Improved Radiation Cooling

The major heat input to the anode takes place in the arc foot region, which is located near location 5″ in Fig. 4. The heat flows in a radial direction toward the thrustor housing and is dissipated by radiation on the front face and the cylindrical section of the housing. Chronic failures were encountered during the first phase of the program because of local overheating and subsequent erosion of the anode insert. The operating life achieved with the original thrustor varied between 4 and 25 hr.

The failures were traced to the press fit between the anode insert and housing. Marks of metal-to-metal contact revealed that only a small percentage of the total area had surface contact; hence, the connection acted as a thermal barrier. It is impractical to eliminate the anode insert by machining the required contour out of one solid piece when using molybdenum or tungsten. Therefore, new methods were conceived to provide a better heat conduction. One solution, which proved to be successful, was the extended anode concept with a radiation disk as shown in Fig. 2. The heat generated in the arc foot region is conducted to the disk, which acts as a heat sink, and the heat is dissipated by radiation from the surface of the disk to the environment. The dimensions of the disk were established analytically by calculating the radiation area required to keep the surface temperature in the hot-spot region below the melting temperature of the material.

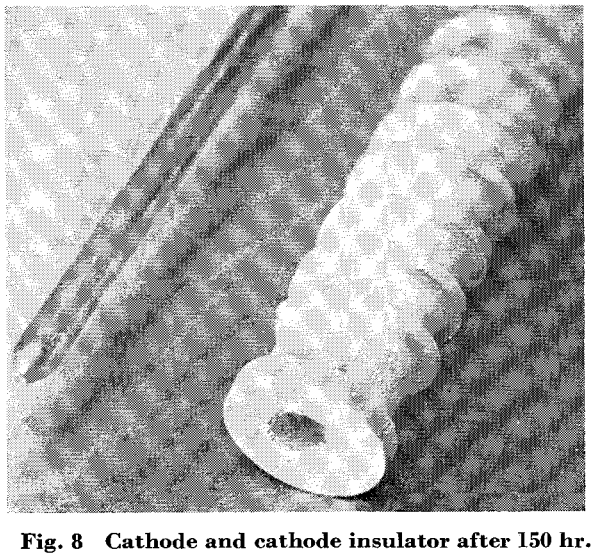

Fig. 8 Cathode and cathode insulator after 150 hr.

Continuous Performance of 2-kw Arc-Jet Thrustor

The thrustor used for this test was that described in the previous section. The time-averaged operating conditions for the 150-hr test run were as follows: hydrogen flow rate, 3.2×10^{-5} lb/sec; hydrogen inlet pressure, 27 psia; thrust, 3.01×10^{-2} lb; specific impulse, 935 sec; efficiency, 30.7%; power input, 2.0 kw.

Peak performance occurred at the 108-hr mark of the continuous test. The values of the parameters at the peak were as follows: hydrogen flow rate, 3.23×10^{-5} lb/sec; thrust, 3.14×10^{-2} lb; specific impulse, 973 sec; efficiency, 33.4%; power input, 2.0 kw.

The test was voluntarily terminated at the end of 150 hr. The temperatures of the anode and the housing were measured with an optical pyrometer throughout the test. The average values of these temperatures were as follows: anode, 1300°C; housing, 1080°C.

Although variation was noted in the values of the anode and housing temperatures during the test, the temperature differential between the anode and the housing remained essentially constant over the entire test run. Maximum thrust and efficiency were obtained when the arc voltage was at a maximum, and when the anode and housing temperatures were at a minimum. Since propellant mass flow was an externally controlled independent variable, this parameter did not enter into these comparisons. It was also observed over relatively short intervals of time that the thrust, specific impulse, and efficiency were at a maximum when the propellant pressure at the inlet to the thrustor was at a minimum.

During the high-voltage period of operation, it is probable that the arc was being stretched out well into the divergent section of the nozzle with the anode attachment region located on the nozzle wall downstream of the throat. These arc conditions were all conducive to transferring a maximum of usable energy to the gas while dissipating a minimum amount of thermal energy in the anode, thereby producing maximum values of thrust, specific impulse, and efficiency for fixed input power level and propellant flow rate. The lower arc current (as measured on the ammeter) contributes by decreasing the fraction of the total input power dissipated in the anode drop region.

The fact that the higher arc voltage was associated with the longer arc length was further substantiated by visual observation. During periods when the voltage was in excess of

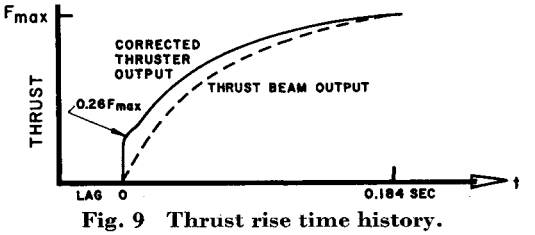

Fig. 9 Thrust rise time history.

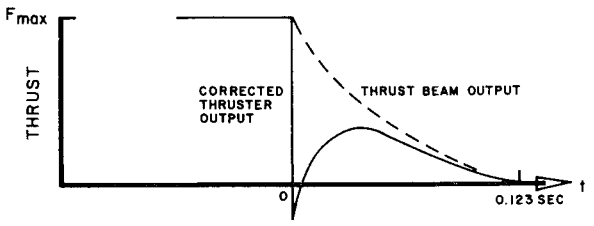

Fig. 10 Thrust decay time history.

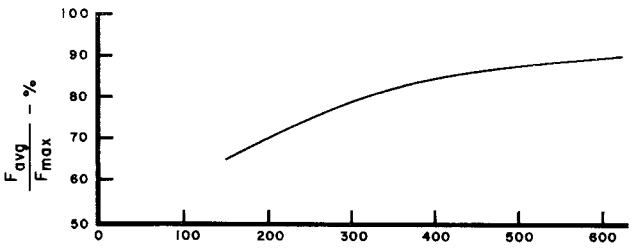

Fig. 11 Ratio of pulsed performance to steady-state performance as a function of pulse width.

100 v, the arc footpoint appeared to be located in the divergent section of the nozzle, and arc operation was very stable. At other times the movement of the anode footpoint of the arc was erratic, and periodically the anode footpoint would relocate inside the throat section reducing the arc voltage and increasing the anode temperature. The relocation of the anode footpoint of the arc was visually observed during operation of the thrustor. It appeared that each successive movement of the anode footpoint of the arc from the low-voltage position to the high-voltage location was accompanied by expulsion of a small quantity of vaporized material, probably from the anode. The lower chamber pressure at the higher voltages would be expected from the previous observations on the location of the arc footpoint.

After this endurance test, the cathode was found to have been reduced in length by 0.041 in. with a consequent weight loss of 0.024 g. The throat diameter of the anode had increased from 0.035 in. at the start of the test to a final average value of 0.0415 in. Figure 8 shows an enlargement of the cathode and its insulator after completion of this test. The cathode tip eroded, and a small cavity was formed in the center of the rod. The BN insulator was eroded slightly at the end closest to the arc and had a slight spongy appearance, probably caused by the vaporization of the binder in the boron nitride material.

A thrustor of the same design was operated at higher power levels in order to determine the maximum specific impulse obtainable with this particular design. The results were as follows: hydrogen flow rate, 2.56×10^{-5} lb/sec; thrust, 3.26×10^{-2} lb; specific impulse, 1270 sec; efficiency, 25.9%; power input, 3.5 kw.

This high specific impulse performance is considered to be representative for this radiation-cooled thrustor design; I_{sp}'s approaching 1270 sec were achieved over a range of power levels and propellant flow rates. Reduction of the mass flow rate of the propellant below approximately 2.5×10^{-5} lb/sec resulted in erratic thrustor operation and erosion of the anode; this can be traced to the fact that the propellant injection system was designed for a hydrogen flow of 3.0×10^{-5} lb/sec, and improper vortex action was obtained when the flow rate was reduced significantly below the designed value. Although this particular thrustor design is sensitive to the flow rate of propellant, an insensitivity to the level of power input was observed in these tests. The same thrustor provided satisfactory performance from 2.0 to 3.5 kw without serious degradation of the thrustor.

Operation of 1-kw Thrustor in Pulsed Mode

A limited series of tests has been run on a 1-kw thrustor in order to determine some of the characteristics of starting and stopping transients and of pulsed-mode operation. A relatively high-response thrust beam was used to measure the transient thrust output. Measured thrust vs time data were corrected to close approximations of actual values using experimentally determined transfer functions of the thrust beam.

Pulse durations as short as 100 msec have been achieved with a fully developed hot jet. Pulse durations in the 300 to 500 msec range produced performance within 80 to 90% of steady-state performance values. Starting and stopping transients were measured and indicated a rise time to full thrust of approximately 185 msec from initiation of the "on" signal and a fall time of 123 msec from initiation of the "off" signal. The thrust rise time and thrust decay time are displayed graphically in Figs. 9 and 10. The lag indicated in Fig. 9 is the time differential between the initiation of the command signal and the first indication of thrust from the arc-jet engine. The experimentally determined transfer functions of the thrust beam were employed to correct the thrust beam output as indicated in Figs. 9 and 10.

The ratio of average thrust to maximum thrust is plotted in Fig. 11 as a function of pulse width. The calculated ratios of average to maximum thrust shown in Fig. 11 can also be representative of the ratios of the average to maximum specific impulse for the pulse, if the assumption of constant propellant flow rate over the pulse duration is reasonably valid. In a preliminary endurance test, 17,580 hot thrust pulses were achieved out of 18,401 commanded pulses (95.5% reliability) before the test was voluntarily terminated. It is to be emphasized that all of the data presented on pulsed-mode operation were obtained from a thrustor designed for steady-state operation. Improved reliability and response time could be expected from a thrustor designed specifically to operate in a transient pulsed condition.

References

[1] Greco, R. V. and Stoner, W. A., "Research and development of a 1-kw plasmajet thruster," AIAA J. **1**, 320–324 (1963).

[2] Ducati, A. C., Humpal, H., Meltzer, J., Muehlberger, E., Todd, J. P., and Waltzer, H., "1-kw arcjet-engine system-performance test," J. Spacecraft Rockets **1**, 327–332 (1964).

[3] Marchand, F. E., Arthur, P. D., and McCoughey, O. J., "Results of satellite raising and orbit transfer studies for low power electrothermal arc-jet propulsion systems," AIAA Preprint 63010 (1963).

[4] "Application studies of low power arc-jet engines for attitude control, station keeping, orbit transfer, and related uses," Plasmadyne Final Rept. FR112–2544 Contract NAS 8-2544 (to be published).

[5] Rouse, H. and Hsieh-Ching Hsu, "On the growth and decay of a vortex filament," Iowa Institute of Hydraulic Research.